Journal of Power Sources 253 (2014) 98–103

Contents lists available at ScienceDirect

Journal of Power Sources

journal homepage: www.elsevier.com/locate/jpowsour

Short communication

Nanowire $Na_{0.35}MnO_2$ from a hydrothermal method as a cathode material for aqueous asymmetric supercapacitors

B.H. Zhang [a,b], Y. Liu [a,b], Z. Chang [a], Y.Q. Yang [a], Z.B. Wen [b,*], Y.P. Wu [a,*], R. Holze [c,*]

[a] New Energy and Material Laboratory (NEML), Department of Chemistry, Fudan University, Shanghai 200433, China
[b] College of Chemistry and Chemical Engineering, Jiangxi Normal University, Nanchang 330022, China
[c] Technische Universität Chemnitz, Institut für Chemie, AG Elektrochemie, D-09107 Chemnitz, Germany

HIGHLIGHTS

- Nanowire $Na_{0.35}MnO_2$ was prepared by a hydrothermal method at low temperature: 205 °C.
- Its electrochemical performance as cathode for aqueous asymmetric supercapacitors was studied.
- Its specific capacitance is (157 F g^{-1}) is much higher than that (92 F g^{-1}) of rod-like $Na_{0.95}MnO_2$ from solid phase reaction.
- The energy density based on AC and nanowire $Na_{0.35}MnO_2$ is 42.6 Wh kg^{-1} at a power density of 129.8 W kg^{-1}.
- The device presents excellent cycling performance even when dissolved oxygen is not removed.

ARTICLE INFO

Article history:
Received 7 August 2013
Received in revised form
16 November 2013
Accepted 3 December 2013
Available online 13 December 2013

Keywords:
Supercapacitor
$Na_{0.35}MnO_2$
Cathode
Hydrothermal method
Aqueous electrolyte

ABSTRACT

Nanowire $Na_{0.35}MnO_2$ was prepared by a simple and low energy consumption hydrothermal method; its electrochemical performance as a cathode material for aqueous asymmetric supercapacitors in Na_2SO_4 solution was investigated. Due to the nanowire structure its capacitance (157 F g^{-1}) is much higher than that of the rod-like $Na_{0.95}MnO_2$ (92 F g^{-1}) from solid phase reaction although its sodium content is lower. When it is assembled into an asymmetric aqueous supercapacitor using activated carbon as the counter electrode and aqueous 0.5 mol L^{-1} Na_2SO_4 electrolyte solution, the nanowire $Na_{0.35}MnO_2$ shows an energy density of 42.6 Wh kg^{-1} at a power density of 129.8 W kg^{-1} based on the total weight of the two electrode material, higher than those for the rod-like $Na_{0.95}MnO_2$, with an energy density of 27.3 Wh kg^{-1} at a power density of 74.8 W kg^{-1}, and that of $LiMn_2O_4$. The new material presents excellent cycling behavior even when dissolved oxygen is not removed from the electrolyte solution. The results hold great promise for practical applications of this cathode material since sodium is much cheaper than lithium and its natural resources are rich.

1. Introduction

Global warming has forced mankind in recent years to explore many methods to protect the environment such as environmentally friendly electric and hybrid electric vehicles. It is well-known that lithium ion batteries can be used for electric vehicles owing to their advantages such as large energy density [1–6]. If electric vehicles are widely used, available lithium sources may turn out to be insufficient. Consequently exploring other kinds of energy storage systems independent of lithium is of great importance. Sodium is similar to lithium. It is not only cheaper but also plentiful in natural resources. Consequently, several sodium-based energy storage devices have been reported [7–12].

Supercapacitors can deliver much higher power density and possess a much longer cycling life than lithium ion batteries. They can be a good complement to lithium ion batteries, which do not show very high power density. Traditional materials such as MnO_2 [13–15], vanadium oxides [16–18] and MoO_3 [19–21] have attracted great attention as cathode materials for aqueous solution-based supercapacitors [22]. However, during charge and discharge processes, these electrodes need cations and anions from the electrolyte, which will affect the ionic conductivities of the electrolytes. In addition, the required amount of electrolyte will be very high, which leads to a decrease of practical energy density. For example, in the case of $VO_x \cdot yH_2O$ [23], a concentration of LiCl solution up to 14 mol L^{-1} was used.

* Corresponding authors.
E-mail addresses: wenzubiao@163.com (Z.B. Wen), wuyp@fudan.edu.cn (Y.P. Wu), rudolf.holze@chemie.tu-chemnitz.de (R. Holze).

0378-7753/$ – see front matter © 2013 Elsevier B.V. All rights reserved.
http://dx.doi.org/10.1016/j.jpowsour.2013.12.011

Recently, aqueous supercapacitors based on alkali-metal intercalation compounds were found [24–29]. During the charge process, these intercalation compounds can provide cations (M^+: M = Li, Na or K), which come to the anode via the aqueous solution. During the discharge process, the cations come back again to the cathode via the aqueous solution. As a result, the concentration and the ionic conductivity of the aqueous electrolyte solution are very stable during the charge and discharge process. The amount of electrolyte will be much smaller than those for symmetric supercapacitors, leading to higher utilization of the electrode materials and higher practical energy density [21]. In addition, the electrolytes are neutral, which is more environmentally friendly than those for symmetric capacitors.

Previously we reported on a cheap cathode material for this kind of aqueous supercapacitor, $NaMnO_2$ [24]. However, the as-prepared products are composed of many small plates and particles, and most of them aggregate together to form large spherical particles with an average diameter of about 50 μm. The energy density of the asymmetric supercapacitor can be 19.5 Wh kg^{-1} at a power density of 130 W kg^{-1} and 13.2 Wh kg^{-1} at 1 kW kg^{-1} [24]. If the redox reaction of $NaMnO_2$ can be fully utilized, evidently its energy density can be higher. It has been acknowledged that nanostructuring is an effective way to improve the efficiency and rate capability of electrode materials [22,28–30]. In this work, we prepared a nanowire $Na_{0.35}MnO_2$ by a simple and low energy consumption hydrothermal method and studied its electrochemical properties as a cathode material (positive mass) for an aqueous symmetric supercapacitor. Its capacitance is much larger than that of the rod-like $Na_{0.95}MnO_2$ from solid-state reaction although the amount of Na is much lower. It presents excellent cycling behavior in the aqueous electrolyte even without removing the dissolved oxygen during assembly. The rate capability is also good.

2. Experimental

All reagents were of analytical grade. At first, nanowire birnessite-MnO_2 (δ-MnO_2) was hydrothermally synthesized by reacting solutions of $MnSO_4$, $(NH_4)_2S_2O_8$ and $(NH_4)_2SO_4$ in a molar ratio of 1:1:4 at 140 °C. Then, nanowire $Na_{0.35}MnO_2$ was prepared by a hydrothermal method [31], which needs much less energy than the traditional solid-state reactions at high temperature. Typically, 0.2 g of the above prepared δ-MnO_2 powder was dispersed in 35 mL of 5 mol L^{-1} NaOH aqueous solution. This solution was placed in a Teflon-lined autoclave (50 mL). The autoclave was heated at 205 °C for 48 h. After that, the precipitated powder was filtered, washed with water three times, and then dried at 60 °C. For comparison, a rod-like $Na_{0.95}MnO_2$ was synthesized using a solid-state reaction. In detail, Na_2CO_3 and the prepared δ-MnO_2 (molar ratio of 1:2) were mixed by ball-milling for 12 h, followed by heating at 870 °C for 10 h under air, which is similar to our previously reported heat-treatment process [24].

The obtained products were characterized using a Bruker Advance 8 powder X-ray diffractometer (XRD) with monochromatized Cu K_α-radiation (λ = 1.54056 Å). SEM micrographs were obtained with a Philip XL30 microscope operated at 25 kV. Elemental analysis was obtained by Thermo E. IRIS Duo inductively coupled plasma (ICP) by dissolving all the materials in concentrated nitric acid solution. N_2 adsorption–desorption isotherms were collected on a Micromeritics ASAP 2010 adsorption analyzer at 100 °C ($Na_{0.35}MnO_2$) and 200 °C ($Na_{0.95}MnO_2$), and the BET specific surface area was calculated.

The cathode was prepared by pressing a powdered mixture of $Na_{0.35}MnO_2$ or $Na_{0.95}MnO_2$, acetylene black and poly(tetrafluoroethylene) (PTFE) in a weight ratio of 8:1:1 onto nickel grid. Activated carbon (AC) from Ningde Xinseng (Chemical Industrial

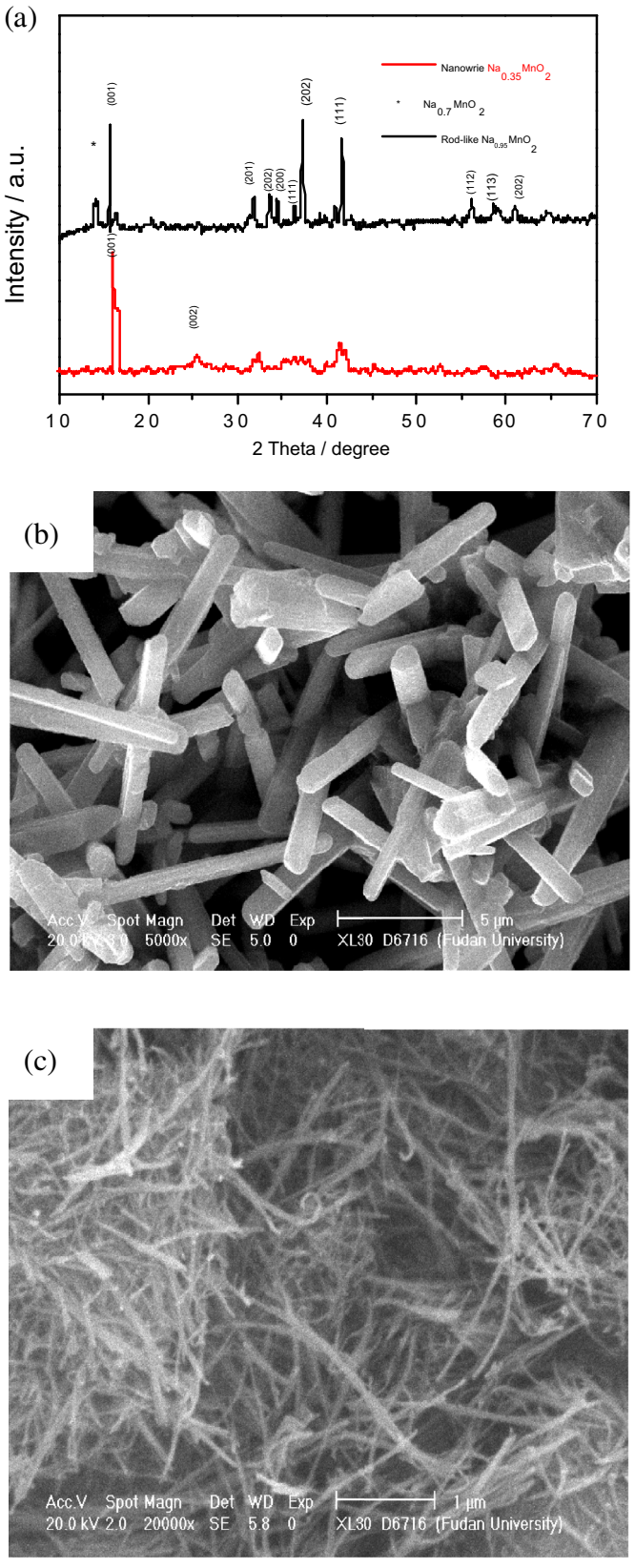

Fig. 1. (a) XRD and (b and c) SEM micrographs of the rod-like $Na_{0.95}MnO_2$ and the nanowire $Na_{0.35}MnO_2$.

Ltd., Co.) with a specific BET-surface area of about 2800 $m^2\ g^{-1}$ was used as received. The AC electrode was prepared in the same way as the cathode. The aqueous Na_2SO_4 solution of 0.5 mol L^{-1} was used as the electrolyte.

Cyclic voltammetric (CVs) tests were done with a three-electrode cell, in which a saturated calomel electrode (SCE) and Ni-grid were used as the reference and the counter electrodes, respectively. Galvanostatic charge–discharge performance was verified using a two-electrode cell. The capacitance was calculated based on the weight of the active cathode material, and the energy density was calculated based on the total weight of two electrodes.

The specific discharge capacity C (F g^{-1}) is calculated according to the following Equation (1) [17,18]:

$$C = (I\Delta t)/(m\Delta V) \quad (1)$$

where I is the applied working current, Δt represents the discharge time, ΔV (V) is the voltage range, and m (g) is the mass of active materials. It can also be expressed in mAh g^{-1}, which is directly calculated according to the following Equation (2).

$$C = (I\Delta t)/m \quad (2)$$

3. Results and discussion

The ICP analysis results show that the molar ratios of Na to Mn for the product from the hydrothermal method is 0.35 and that from the solid-state method is 0.95, respectively. The XRD patterns of the prepared $Na_{0.35}MnO_2$ and $Na_{0.95}MnO_2$ are shown in Fig. 1(a). The peaks at about 17.1° and 25° are assigned to the diffraction of (001) and (002) planes, respectively, indicating the layered structure of $Na_{0.35}MnO_2$ [32]. In comparison, the XRD pattern of $Na_{0.95}MnO_2$ is almost identical to that reported in the JCPDS data (JCPDS file No. 25-0845), there is only a small amount of the $Na_{0.7}MnO_2$ phase impurity (JCPDS file No. 27-0751), which can be identified from the peak at 15.8°.

SEM micrographs of $Na_{0.35}MnO_2$ and $Na_{0.95}MnO_2$ are shown in Fig. 1b and c. It can be observed that the prepared $Na_{0.35}MnO_2$ has a nanowire structure, with 30 nm in width. However, $Na_{0.95}MnO_2$ has a coarser rod morphology, with about 5 μm in length and 500 nm in width, much larger than the dimensions of the $Na_{0.35}MnO_2$ nanowire.

CVs of AC, the prepared $Na_{0.35}MnO_2$ and $Na_{0.95}MnO_2$ in 0.5 mol L^{-1} Na_2SO_4 aqueous electrolyte in the three-electrode cell with nickel mesh as the counter electrode at the scan rate of 5 mV s^{-1} are shown in Fig. 2(a). The CV of an AC electrode shows an ideal rectangular shape without any noticeable redox peaks from 0.1 to −0.8 V (vs. SCE), which is characteristic of charging/discharging of the double layer capacitance [33,34]. The nanowire $Na_{0.35}MnO_2$ shows two clearly separated sharp redox peaks corresponding to the intercalation/de-intercalation of Na^+ ions [35]. Two oxidation peaks located at 0.62 and 0.82 V (vs. SCE), respectively, can be seen clearly, whereas, there is only one clear reduction peak located at 0.29 V (vs. SCE), which is probably due to that the overlapping of two reduction peaks. The behavior of the $Na_{0.95}MnO_2$ electrode slightly deviates from the ideal rectangular shape with two small redox couples, indicative of both the capacitive and the pseudocapacitive property of the $Na_{0.95}MnO_2$ cathode, whose two oxidation peaks are located at 0.58 and 0.82 V (vs. SCE) and two reduction peaks at 0.29 and 0.51 V (vs. SCE), respectively. The peak separation for the redox peaks is a little larger compared

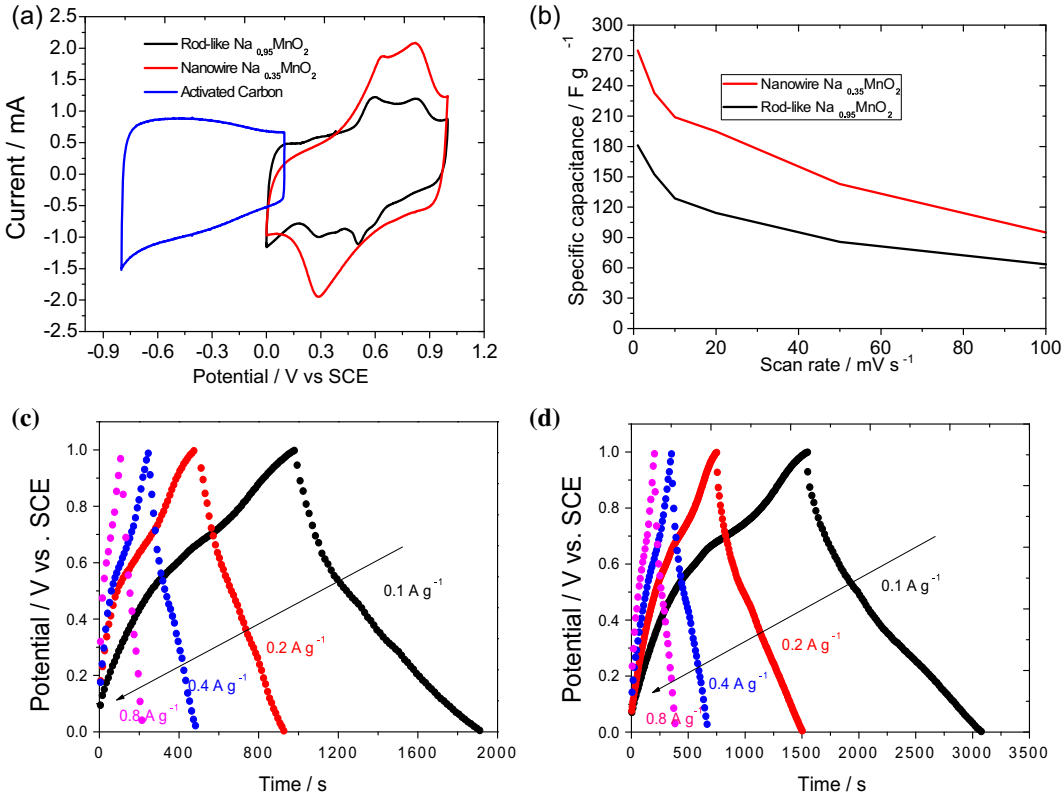

Fig. 2. (a) Cyclic voltammograms of AC the nanowire $Na_{0.35}MnO_2$ and the rod-like $Na_{0.95}MnO_2$ electrode in 0.5 mol L^{-1} Na_2SO_4 aqueous solution at a scan rate of 5 mV s^{-1}, (b) specific capacitance against the scan rate of CV for the rod-like $Na_{0.95}MnO_2$ and the nanowire $Na_{0.35}MnO_2$, and the potential–time curves for (c) the rod-like $Na_{0.95}MnO_2$ and (d) the nanowire $Na_{0.35}MnO_2$ at the current densities from 0.1 to 0.8 A g^{-1} at the potential range of 0–1.0 V (vs. SCE).

to the reported [36]. Perhaps it is due to different test cells. However, the area for the CV-curve of the nanowire $Na_{0.35}MnO_2$ is larger than that of the rod-like $Na_{0.95}MnO_2$, indicating that the capacitance of the former will be larger though its content of sodium is lower.

The change of the specific capacitance with the scan rate CV is shown in Fig. 2(b). From the CV test, the capacitances for the nanowire $Na_{0.35}MnO_2$ and the rod-like $Na_{0.95}MnO_2$ can be up to 275 and 180 F g^{-1}, respectively, at the low scan rate. It is similar to the reported results that the capacitance fades with the increase of the scan rate [27,28,33]. The potential–time curves at different current density from 0.1 to 0.8 A g^{-1} for the nanowire $Na_{0.35}MnO_2$ and the rod-like $Na_{0.95}MnO_2$ (Fig. 2(c) and (d)) show that the capacitance fades with the current density. However, the fading is not much.

Charge and discharge curves and cycling behavior for AC, the nanowire $Na_{0.35}MnO_2$ and the rod-like $Na_{0.95}MnO_2$ at 200 mA g^{-1} are shown in Fig. 3. The AC-based symmetric supercapacitor presents smaller energy density in neutral aqueous electrolyte [33,37]. Both supercapacitors based on the nanowire $Na_{0.35}MnO_2$ and the rod-like $Na_{0.95}MnO_2$ do not show sharp or linear charge and discharge curves due to the existence of the pseudo-capacitance from the redox reactions and double-layer electric capacitance, which is consistent with the results from the CV curves. Especially the nanowire $Na_{0.35}MnO_2$ presents a clear voltage platform during the charge and discharge process. The capacitance of $Na_{0.35}MnO_2$ (157 F g^{-1}) is higher than that of $Na_{0.95}MnO_2$ (92 F g^{-1}) though the sodium content in the former is much less than that in the latter. This can be mainly ascribed to two reasons: (1) the nanowire structure of the $Na_{0.35}MnO_2$, which greatly shortens the distance for the de-intercalation and intercalation of Na^+-cations, and (2) the larger surface area measured from BET method for the $Na_{0.35}MnO_2$ (86.7 m^2 g^{-1}), which provides more Na^+ ions or sites at the surface of the layer structured $NaMnO_2$ than that of $Na_{0.95}MnO_2$ (3.48 m^2 g^{-1}). Their capacitances are larger than those of our formerly reported $NaMnO_2$ of 38.9 F g^{-1} [23], which is also due to smaller particle size and larger surface area. Both present excellent cycling and their capacitances do not fade evidently after 5000 cycles even when the oxygen in the aqueous solution is not removed, which suggest superior electrochemical performance of these cathode materials for symmetric capacitors in the aqueous solutions [21]. In addition, both of them show a Coulombic efficiency of nearly 100% except in the first several cycles, indicative of a good electrochemical stability.

The Nyquist plots obtained from the nanowire $Na_{0.35}MnO_2$ and the rod-like $Na_{0.95}MnO_2$ using Ni mesh as the counter electrode are shown in Fig. 4. It can be seen clearly that the charge-transfer resistance of the nanowire $Na_{0.35}MnO_2$ is lower than that of the rod-like $Na_{0.95}MnO_2$ indicating that the rate capability of the nanowire $Na_{0.35}MnO_2$ will be better than that of the rod-like $Na_{0.95}MnO_2$, which is evidently due to the nanowire structure and the higher surface area of the nanowire $Na_{0.35}MnO_2$. Though the data of the charge-transfer resistance of both electrodes are higher than some other reported materials such as Mn_3O_4 [38], it is perhaps due to different cell configuration. From the following, it can be seen that the rate capability is still very good.

The charge and discharge curves of the asymmetric supercapacitors AC/0.5 mol L^{-1} Na_2SO_4/$Na_{0.35}MnO_2$ ($Na_{0.95}MnO_2$), Ragone plots of the asymmetric supercapacitors AC/0.5 mol L^{-1} Na_2SO_4/$Na_{0.35}MnO_2$ ($Na_{0.95}MnO_2$) and the symmetric supercapacitors AC/0.5 mol L^{-1} Na_2SO_4/AC are shown in Fig. 5. The charge and discharge curves of the supercapacitors are similar to those of their cathode materials, which do not present a linear shape. This is due to the pseudo-capacitance of the redox reactions from the cathode. Of course, the weight ratio of the electrodes largely affects the electrochemical performance for asymmetric supercapacitors. To get a good balance for the capacitance, the gravimetric ratios of the asymmetric supercapacitors are optimized and the weight ratio for AC/$Na_{0.35}MnO_2$ and AC/$Na_{0.95}MnO_2$ are 1:1.3 and 1.3:1, respectively. The asymmetric supercapacitor AC/

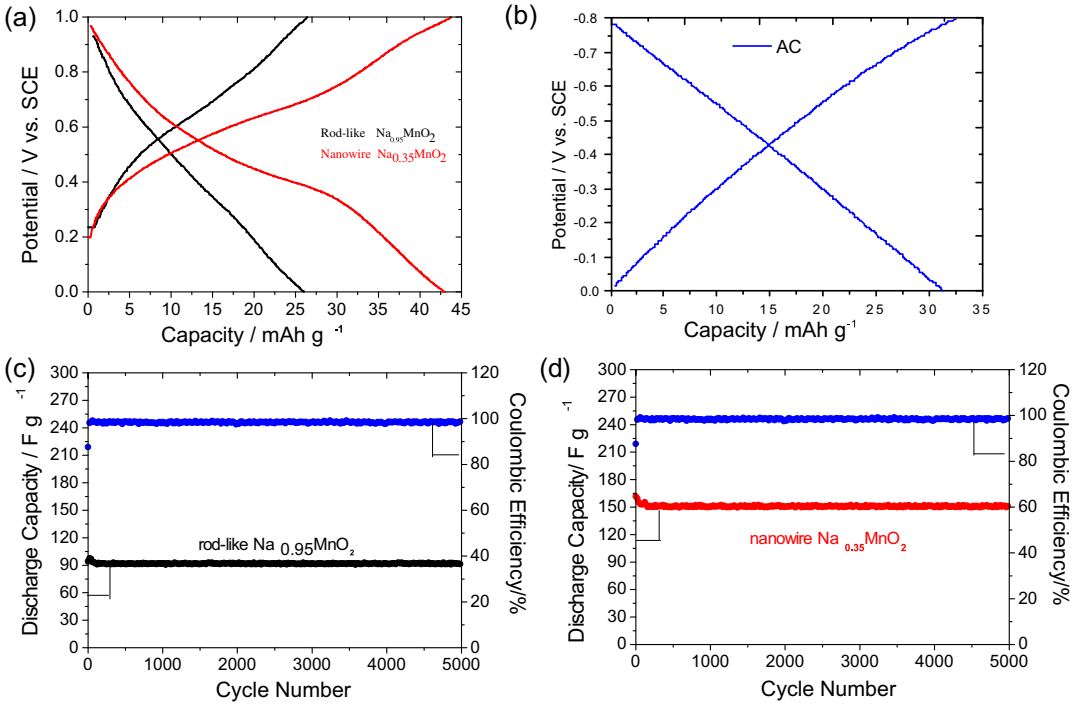

Fig. 3. Charge-discharge profiles of (a) the rod-like $Na_{0.95}MnO_2$ and nanowire $Na_{0.35}MnO_2$ between 0 and 1 V and (b) AC anode between −0.8–0 V (vs. SCE) at 200 mA g^{-1}, Ni as electrode and SCE as reference electrode, and cycling performance and Coulombic efficiency of (c) the rod-like $Na_{0.95}MnO_2$ (d) the nanowire $Na_{0.35}MnO_2$.

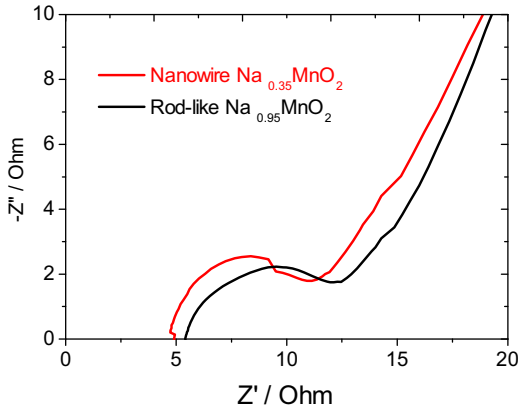

Fig. 4. Nyquist plots for the nanowire $Na_{0.35}MnO_2$ and the rod-like $Na_{0.95}MnO_2$ measured after their immersion in the electrolyte for three hours.

0.5 mol L^{-1} Na_2SO_4/$Na_{0.35}MnO_2$ shows an energy density of 42.6 Wh kg^{-1} at a power density of 129.8 W kg^{-1}, higher than that of the supercapacitor AC/0.5 mol L^{-1} Na_2SO_4/$Na_{0.95}MnO_2$ that only delivers an energy density of 27.3 Wh kg^{-1} at a power density of 74.8 W kg^{-1}. The symmetric supercapacitors AC/0.5 mol L^{-1} Na_2SO_4/AC shows an energy density of 5.6 Wh kg^{-1} at a power density of 51.5 W kg^{-1} [33]. Its energy density does not fade as fast as the asymmetric supercapacitors. When the power density increases, their energy density decreases. However, the nanowire $Na_{0.35}MnO_2$ presents higher energy density than the rod-like $Na_{0.95}MnO_2$. The main reasons are ascribed to the nano structure and the larger surface area of the $Na_{0.35}MnO_2$, which are consistent with the former results. Since their capacitances are higher than that of our formerly reported $NaMnO_2$, their energy densities are also higher.

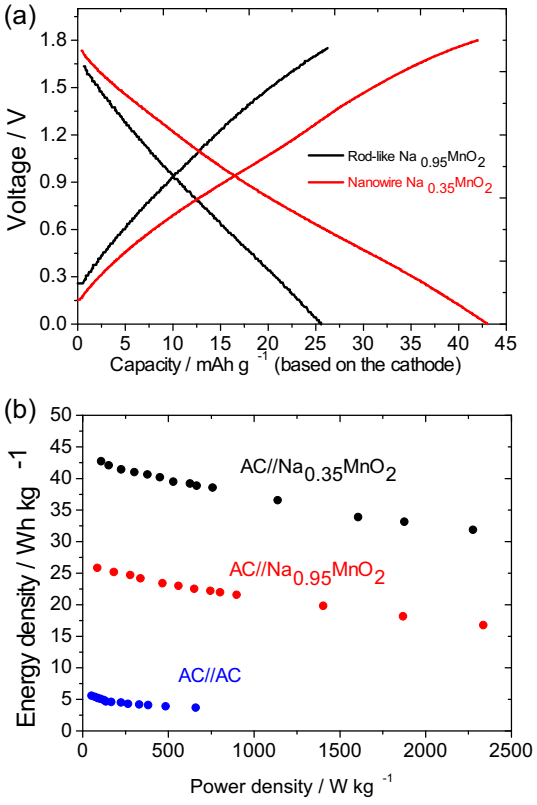

Fig. 5. (a) Charge–discharge profiles for 500th cycles of the rod-like $Na_{0.95}MnO_2$ and the nanowire $Na_{0.35}MnO_2$ at a current density of 200 mA g^{-1} between 0 and 1.8 V, AC as electrode and reference electrode (b) Ragone plots of capacitor AC//AC, and supercapacitors of AC//nanowire $Na_{0.35}MnO_2$ and AC//trod-like $Na_{0.95}MnO_2$.

4. Conclusions

For the first time we used a hydrothermal method to prepare a nanowire $Na_{0.35}MnO_2$. It presents better electrochemical behavior than the rod-like $Na_{0.95}MnO_2$ from the solid-state method as the cathode for an asymmetric supercapacitor using activated carbon as the anode and 0.5 mol L^{-1} Na_2SO_4 aqueous solution as the electrolyte. The capacitance of the nanowire $Na_{0.35}MnO_2$ (157 F g^{-1}) is much higher than that of the rod-like $Na_{0.95}MnO_2$ (92 F g^{-1}). It presents excellent cycling performance even when the oxygen in the aqueous electrolyte is not removed; and no evident capacitance fading after 5000 cycles. The nanowire $Na_{0.35}MnO_2$ delivers an energy density 42.6 Wh kg^{-1} (based on the total mass of the active electrode materials) at a power density of 129.8 W kg^{-1} with activated carbon as the anode, higher than that of the rod-like $Na_{0.95}MnO_2$, 27.3 Wh kg^{-1} at a power density of 74.8 W kg^{-1} and that of $LiMn_2O_4$. Beyond providing an easy synthesis method for layered $Na_{0.35}MnO_2$ with high capacitance this work shows promise for the application in electric vehicles due to its low price and environmental friendliness.

Acknowledgments

Financial supports from 973 Program (No: 2007CB209702) and STCSM (12JC1401200) are gratefully appreciated.

References

[1] M. Armand, J.-M. Tarascon, Nature 451 (2008) 652–657.
[2] Z. Li, F. Du, X.F. Bie, D. Zhang, Y.M. Cai, X.R. Cui, C.Z. Wang, G. Chen, Y.J. Wei, J. Phys. Chem. C 114 (2010) 22751–22757.
[3] M. Fehse, F. Fischer, C. Tessier, L. Stievano, L. Monconduit, J. Power Sources 231 (2013) 23–28.
[4] J. Liu, H.Y. Xu, X.L. Jiang, J. Yang, Y.T. Qian, J. Power Sources 231 (2013) 39–43.
[5] R.J. Brodd, C. Helou, J. Power Sources 231 (2013) 293–300.
[6] M.M. Thackeray, S.H. Kang, C.S. Johnson, J.T. Vaughey, R. Benedek, S.A. Hackney, J. Mater. Chem. 17 (2007) 3112–3125.
[7] J.F. Whitacre, A. Tevar, S. Sharma, Electrochem. Commun. 12 (2010) 463–466.
[8] P. Senguttuvan, G. Rousse, M.E. de Dompablo, H. Vezin, J.M. Tarascon, M.R. Palacin, J. Am. Chem. Soc. 135 (2013) 3897–3903.
[9] P. Hartmann, C.L. Bender, M. Vracar, A.K. Durr, A. Garsuch, J. Janek, P. Adelhelm, Nat. Mater. 12 (2013) 228–232.
[10] D.D. Yuan, W. He, F. Pei, F.Y. Wu, Y. Wu, J.F. Qian, Y.L. Cao, X.P. Ai, H.X. Yang, J. Mater. Chem. A 1 (2013) 3895–3899.
[11] P. Vassilaras, X.H. Ma, X. Li, G. Ceder, J. Electrochem. Soc. 160 (2013) A207–A211.
[12] Z.G. Yang, J.L. Zhang, M.C.W. Kintner-Meyer, X.C. Lu, D. Choi, J.P. Lemmon, J. Liu, Chem. Rev. 111 (2011) 3577–3613.
[13] W. Tang, Y.Y. Hou, X.J. Wang, Y. Bai, Y.S. Zhu, H. Sun, Y.B. Yue, Y.P. Wu, K. Zhu, R. Holze, J. Power Sources 197 (2012) 330–333.
[14] J. Shao, X.Y. Li, Q.T. Qu, Y.P. Wu, J. Power Sources 223 (2013) 56–61.
[15] Q.T. Qu, P. Zhang, B. Wang, Y.H. Chen, S. Tian, Y.P. Wu, R. Holze, J. Phys. Chem. C 113 (2009) 14020–14027.
[16] J. Shao, X.Y. Li, Q.T. Qu, H.H. Zheng, J. Power Sources 219 (2012) 253–257.
[17] S.D. Perera, A.D. Liyanage, N. Nijem, J.P. Ferraris, J.Y. Chabal, K.J. Balkus Jr., J. Power Sources 230 (2013) 130–137.
[18] Q.T. Qu, Y.S. Zhu, X.W. Gao, Y.P. Wu, Adv. Energy Mater. 2 (2012) 950–955.
[19] W. Tang, L.L. Liu, S. Tian, L. Li, Y.B. Yue, Y.P. Wu, K. Zhu, Chem. Commun. 47 (2011) 10058–10060.
[20] W. Tang, L.L. Liu, Y.S. Zhu, H. Sun, Y.P. Wu, K. Zhu, Energy Environ. Sci. 5 (2012) 6909–6913.
[21] J.B. Jiang, J.L. Liu, S.J. Peng, D. Qian, D.M. Luo, Q.F. Wang, Z.W. Tian, Y.C. Liu, J. Mater. Chem. A 1 (2013) 2588–2594.
[22] F.X. Wang, S.Y. Xiao, Y.Y. Hou, C.L. Hu, L.L. Liu, Y.P. Wu, RSC Adv. 3 (2013) 1039–1044.
[23] J.M. Li, K.H. Chang, C.C. Hu, Electrochem. Commun. 12 (2010) 1800.
[24] Q.T. Qu, Y. Shi, S. Tian, Y.H. Chen, Y.P. Wu, R. Holze, J. Power Sources 194 (2009) 1222–1225.
[25] B.L. Ellis, W.R.M. Makahnouk, Y. Makimura, K. Toghill, L.F. Nazar, Nat. Mater. 6 (2007) 749–753.

[26] Q.T. Qu, L. Li, S. Tian, W.L. Guo, Y.P. Wu, R. Holze, J. Power Sources 195 (2010) 2789–2794.
[27] Q.T. Qu, L.J. Fu, X.Y. Zhan, D. Samuelis, L. Li, W.L. Guo, Z.H. Li, Y.P. Wu, J. Maier, Energy Environ. Sci. 4 (2011) 3985–3990.
[28] F.X. Wang, S.Y. Xiao, Y. Shi, L.L. Liu, Y.S. Zhu, Y.P. Wu, J.Z. Wang, R. Holze, Electrochim. Acta 93 (2013) 301–306.
[29] W. Tang, Y.Y. Hou, F.X. Wang, L.L. Liu, Y.P. Wu, K. Zhu, Nano Lett. 13 (2013) 2036–2040.
[30] Y.G. Guo, Y.S. Hu, W. Sigle, J. Maier, Adv. Mater. 19 (2007) 2087–2091.
[31] Z. Li, D. Young, K. Xiang, W.C. Carter, Y.M. Chiang, Adv. Energy Mater. 3 (2013) 290–294.
[32] H. Matsui, J. Ju, T. Odaira, N. Toyota, J. Phys. Soc. Jpn. 78 (2009), 074801.
[33] Q.T. Qu, B. Wang, L.C. Yang, Y. Shi, S. Tian, Y.P. Wu, Electrochem. Commun. 10 (2008) 1652.
[34] Z.B. Wen, Q.T. Qu, Q. Gao, Z.H. Hu, Y.P. Wu, X.W. Zheng, Y.F. Liu, X.J. Wang, Electrochem. Commun. 11 (2009) 715.
[35] L. Athouel, F. Moser, R. Dugas, O. Crosnier, D. Bélanger, T. Brousse, J. Phys. Chem. C 112 (2008) 7270–7277.
[36] C.T. Hsu, C.C. Hu, J. Power Sources 242 (2013) 662.
[37] T.H. Wu, C.T. Hsu, C.C. Hu, L.J. Hardwick, J. Power Sources 242 (2013) 289.
[38] T.H. Wu, Y.H. Chu, C.C. Hu, L.J. Hardwick, Electrochem. Commun. 27 (2013) 81.